LC Taipei : 7th ACFA Workshop

News on the Electron-Electron Initial State

C.A. Heusch
Univ. of California, Santa Cruz

The ITRP recommendation that the ILC should adopt the Superconducting Technology changes the boundary conditions for using the e^-e^- initial state.

But: it does not detract from the basic fact that this is the only pure initial state:

Charge, Spin, and Polarization are fully defined as well as the Energy.

We mention advantages of the technology choice for experiments starting from e^-e^-.

International Journal of Modern Physics A
Vol. 18, No. 16 (2003) 2827–2833

World Scientific
www.worldscientific.com

LUMINOSITY EXPECTATIONS FOR ELECTRON-ELECTRON COLLISIONS AT TESLA

S. SCHREIBER
Deutsches Elektronen-Synchrotron, 22603 Hamburg, Germany

Electron-electron collisions at the future TESLA linear collider have been studied. Achievable luminosity and luminosity spectra for parameters close to the standard TESLA design are given.

1 Introduction

The TESLA linear collider is designed for e^+e^- collisions at $\sqrt{s} = 500\,\mathrm{GeV}$ and beyond. Basic parameters are given in Tab. 1. Accelerating electrons in both arms of the TESLA collider allows to explore the rich physics potential of e^-e^- interactions.[1] The TESLA proposal includes e^-e^- collision experiments as an option. This report discusses luminosity expectations of e^-e^- collisions in TESLA with parameters close to the standard e^+e^- design. Key points are the achievable luminosity and its stability.

2 Luminosity

For flat beams ($\sigma_y/\sigma_x \ll 1$) the luminosity for $E_{\mathrm{cm}} = 500\,\mathrm{GeV}$ can be expressed as

$$\mathcal{L} = 7.2{\cdot}10^{29}\,\mathrm{cm}^{-2}\mathrm{s}^{-1}\,\frac{\eta P_{\mathrm{AC}}\,[MW]}{\sqrt{\epsilon_y\,[m]}}\,\sqrt{\delta_b}H_D \qquad (1)$$

Table 1. TESLA 500 parameter list.

Parameter	Symbol	Ref. Design
Center of mass energy	E_{cm}	500 GeV
Bunch charge	N	$2{\cdot}10^{10}$ 1/e
Bunches per train	n_b	2820
Bunch spacing	t_b	337 ns
Train current		950 mA
Train length		950 μs
Repetition rate	f_{rep}	5 Hz
Bunch length	σ_z	300 μm
IP Beam size (h/v)	$\sigma_{x,y}$	553, 5 nm
IP beta function (h/v)	$\beta_{x,y}$	15, 0.4 mm
IP emittance (norm.) (h/v)	$\epsilon_{x,y}$	10, $0.03{\cdot}10^{-6}$ m
Vert. divergence at IP	$\sigma_{y'}$	12.3 μrad
Energy loss dp/p (beamstr.)	δ_b	3.3 %
Vertical Disruption	D_y	25
AC power (2 linacs)	P_{AC}	95 MW
Luminosity e^+e^- mode	$\mathcal{L}^{+-}$	$3{\cdot}10^{34}\,\mathrm{cm}^{-2}\mathrm{s}^{-1}$
Luminosity e^-e^- mode	$\mathcal{L}^{--}$	$0.47{\cdot}10^{34}\,\mathrm{cm}^{-2}\mathrm{s}^{-1}$

with P_{AC} the overall AC power consumption, η the AC-to-beam power efficiency, ϵ_y the normalized vertical emittance, and δ_b the average energy loss due to beamstrahlung. TESLA has chosen a reasonable power consumption of $P_{AC} = 95\,\mathrm{MW}$. One advantage of TESLA is the favorable AC-to-beam power efficiency of $\eta = 22\,\%$ due to the use of superconducting accelerating structures.

The enhancement or reduction of the luminosity is described by the factor H_D. It is around 2 for e^+e^- collisions, but for e^-e^- a value around 1/3 is expected due to the repelling forces for like sign charged particles. Unfortunately, there is no complete analytical expression for H_D (see e.g. [7]). Therefore, a simulation of the beam-beam interaction is used to evaluate the luminosity (GUINEA-PIG[5]).

For e^+e^- collisions, the luminosity is increased, if the vertical waists of the colliding beams do not coincide but are shifted away from the interaction point (IP) in longitudinal direction by a small amount. This effect is a consequence of the pinch effect for unlike-sign particles and is expected to be small in the e^-e^- case. Figure 1 shows the luminosity for e^-e^- collisions as a function of the waist shift. The highest luminosity is for the case, when both beams are focused before the IP: by 30 μm for a bunch length of 300 μm and 50 μm for $\sigma_z = 400\,\mu$m.

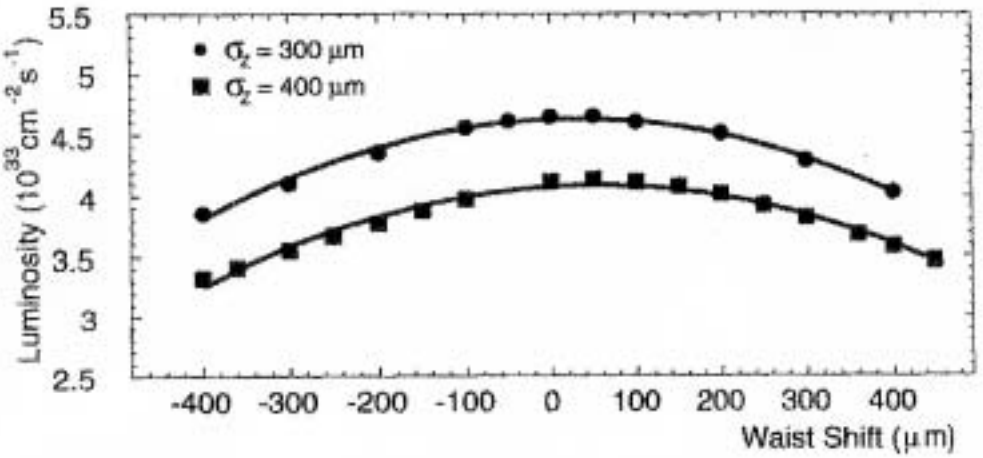

Figure 1. Luminosity of e^-e^- interactions as a function of the shift of both vertical beam waists in longitudinal direction for a bunch length of 300 μm and 400 μm. Parameters from Table 1 have been used.

Since the vertical emittance of $3{\cdot}10^{-8}$ m is already very demanding, Equ. (1) shows, that the only parameters left for tuning the luminosity are the beamstrahlung induced energy loss δ_b and the parameter H_D. In the first case, one has to allow for a larger energy loss δ_b to improve, which has to be acceptable for physics. A larger H_D can be expected by decreasing the vertical disruption D_y. Looking at the analytical expressions for δ_b and D_y, $\delta_b = 0.86\, r_e^3 \gamma N^2/(\sigma_x{}^2\sigma_z)$ and $D_y = 2Nr_e\sigma_z/(\gamma\sigma_x\sigma_y)$, the bunch length σ_z and the horizontal beam size σ_x are adequate parameters to tune. N denotes the bunch charge, r_e the classical electron radius, γ the Lorentz factor, and σ_y the vertical beam sizes at the IP.

Figure 2 shows the luminosity and average energy loss due to beamstrahlung as

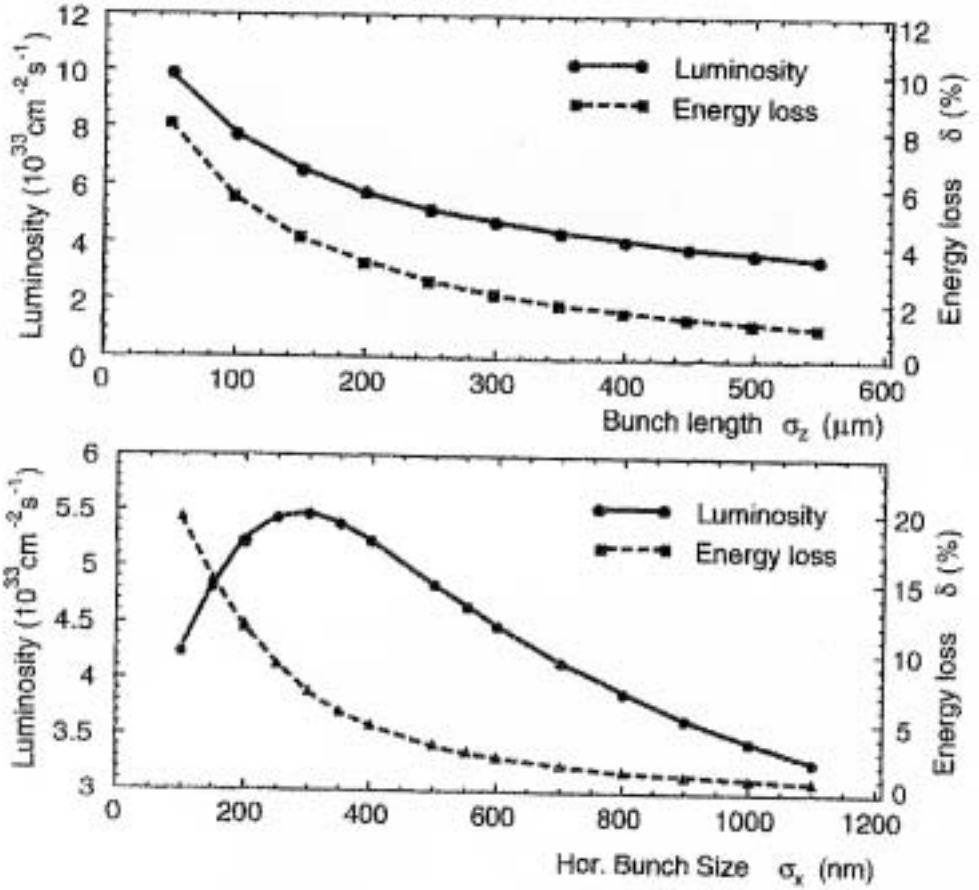

Figure 2. Luminosity and energy loss due to beamstrahlung for e^-e^- collisions as a function of the bunch length and horizontal bunch size. Parameters from Table 1 have been used.

a function of bunch length and horizontal spot size. All calculations are based on TESLA parameters from Table 1 and are summarized in Table 2.

Shorter bunches result in a larger luminosity as expected from the equations above: $\mathcal{L} \propto \sqrt{\delta_b} \propto 1/\sqrt{\sigma_z}$. Reducing the horizontal spot size is also a possibility to enhance the luminosity, since $\mathcal{L} \propto \sqrt{\delta_b} \propto 1/\sigma_x$. However, in contrast to the bunch length, the disruption increases with $D_y \propto 1/\sigma_x$ as well. For large disruption, the repelling forces of the electrons reduce the luminosity. The optimum horizontal spot size for TESLA parameters is around 300 μm. Thus, an additional gain in luminosity is achieved by reducing the horizontal spot size from 553 nm down to 300 μm. The luminosity increases by 14 % to $0.55{\cdot}10^{34}\,\mathrm{cm}^{-2}\mathrm{s}^{-1}$, but δ_b is enlarged significantly to 7.2 %.

A reevaluation of the bunch compressor scheme for TESLA showed, that a compression down to $\sigma_z = 300\,\mu\mathrm{m}$ is possible. This results in an increase of luminosity and in a better performance of the feedback system compared to the previous case of $\sigma_z = 400\,\mu\mathrm{m}$.[2] The e^-e^- luminosity calculated for this case ($\sigma_z = 300\,\mu\mathrm{m}$, $\sigma_x = 553\,\mathrm{nm}$) is $0.47{\cdot}10^{34}\,\mathrm{cm}^{-2}\mathrm{s}^{-1}$ with $H_D = 0.34$ and a beamstrahlung induced energy loss δ_b of 2.2 %. Even shorter bunches and thus an increase of δ_b to up to

Table 2. Luminosity $\mathcal{L}$ and beamstrahlung induced energy loss δ_b for e^-e^- collisions. Standard TESLA parameters of Tab. 1 have been used.

σ_z (μm)	σ_x (nm)	δ_b (%)	$\mathcal{L}$ (10^{33} cm^{-2}s^{-1})
400	553	1.6	4.1
300	553	2.2	**4.7**
200	553	3.3	5.7
100	553	5.6	7.7
50	553	8.1	9.9
300	400	4.8	5.2
300	300	7.2	**5.5**
300	200	12	5.2
300	100	20	4.2

10 % seems to be tolerable for physics given the fact, that the luminosity spectrum for e^-e^- collisions is narrower than the spectrum for e^+e^- (Fig. 3 left). Moreover, a bunch length reduction would not spoil the spectrum significantly (Fig. 3 right).

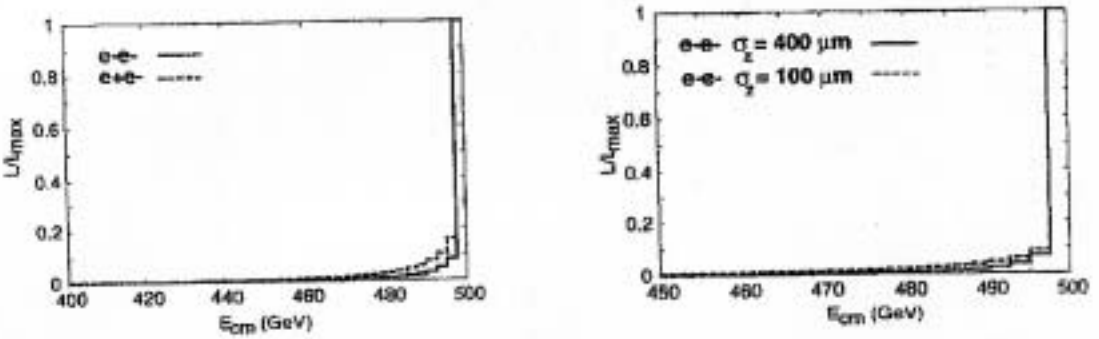

Figure 3. Normalized luminosity spectra for e^-e^- collisions compared to e^+e^- with standard parameters from Tab. 1 (left) and for different bunch lengths (right).

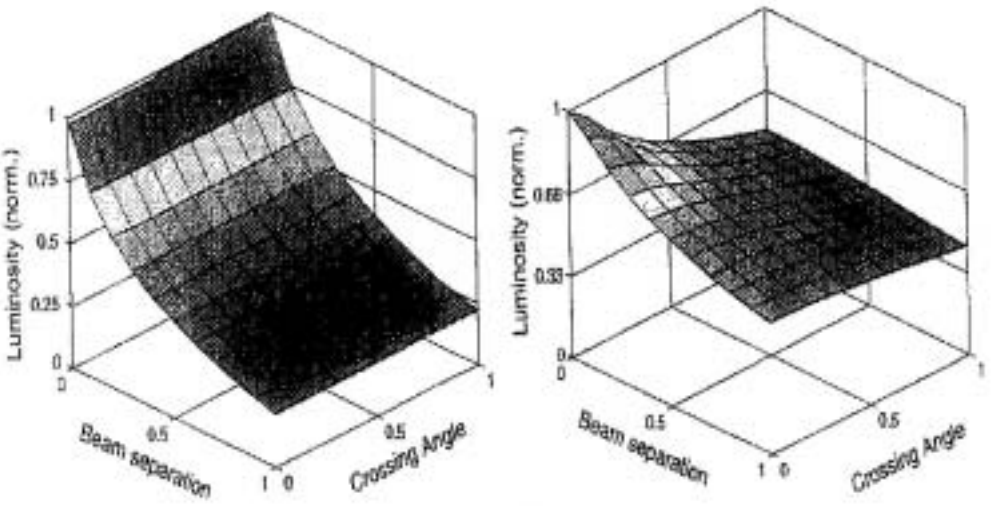

Figure 4. Luminosity as a function of vertical beam separation and crossing angle for the e^-e^- case (left) and the e^+e^- case (right). The luminosity is normalized to allow a relative comparison between both cases. The beam separation is normalized to the IP spot size of $\sigma_y = 5\,\mathrm{nm}$ and the crossing angle to the IP divergence of $\sigma_{y'} = 12.3\,\mu\mathrm{rad}$. TESLA parameters used as listed in Tab. 1.

This system measures the separation of the first bunches in a train, compensates the displacement and maintains the train in collision. A schematic layout of the proposed intra-train feedback system for interactions is shown in Fig. 5 (left). It is described in detail in [2] and is based on a similar system developed for e^+e^- collisions.[4] Due to the strong beam-beam deflection a vertical separation between two electron bunches at the interaction point (IP) becomes detectable, even in a range well below the vertical beam size of 5 nm. The angular kick results in a

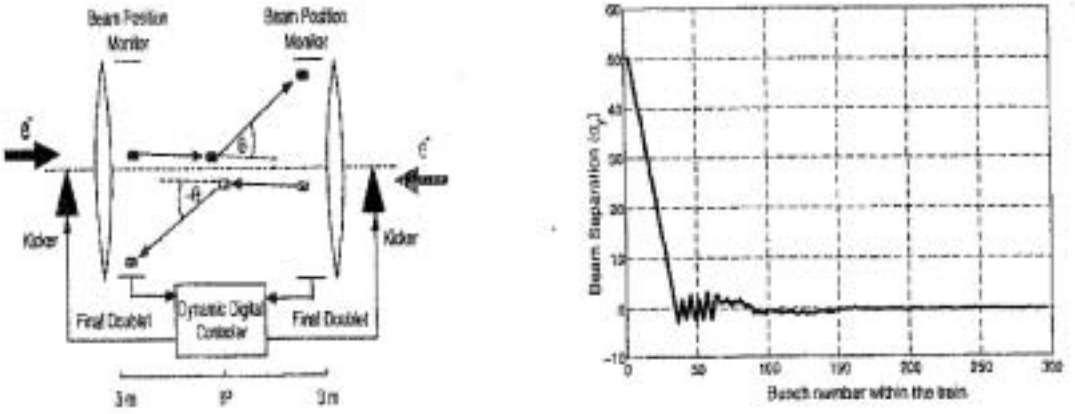

Figure 5. Layout of the e^-e^- feedback system at the interaction point (left). Example of the response of the feedback system with a two model controller (right). The aggressive model brings the beams rapidly into collision. Switching the moderate model after 50 bunches reduces the oscillations and insures a high correction accuracy for the subsequent bunches. Note, that the total number of bunches within a train is 2820.

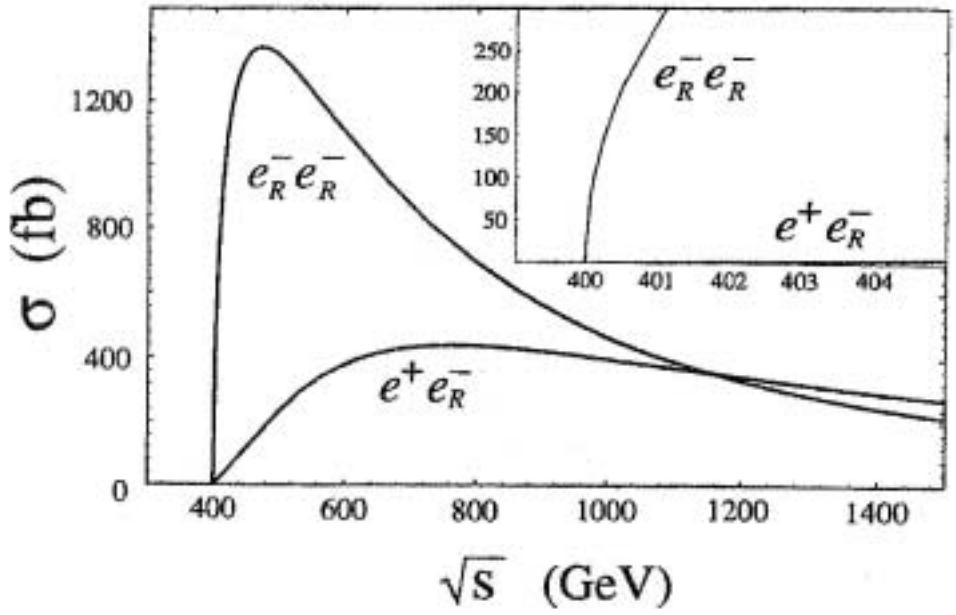

Fig. 2. Cross sections $\sigma(e_R^- e_R^- \to \tilde{e}_R^- \tilde{e}_R^-)$ and $\sigma(e^+ e_R^- \to \tilde{e}_R^+ \tilde{e}_R^-)$ for $m_{\tilde{e}_R} = 200$ GeV and $m_{\tilde{B}} = 100$ GeV. The inset is a magnified view for $\sqrt{s}$ near threshold. Effects of initial state radiation, beamstrahlung, and the selectron width are not included.

$$\Delta m = \Delta\sigma \left(\frac{\partial\sigma}{\partial m}\right)^{-1}, \tag{3}$$

where $\Delta\sigma = \sqrt{\sigma/L}$, and L is the total integrated luminosity. At $\sqrt{s} = 2m_{\tilde{e}_R} + 0.5$ GeV, where the cross section is $\sigma = 200$ fb, an integrated luminosity of $L = 1$ fb^{-1} gives a cross section measurement of $\Delta\sigma = 14$ fb, and the resulting 1σ statistical uncertainty on the mass is $\Delta m = 40$ MeV. This result contrasts sharply with results from the e^+e^- mode, which, as noted above, are typically more than an order of magnitude worse. Note also that the necessary integrated luminosity can be collected in a matter of weeks, even given the possible factor of 2 to 3 reduction in luminosity for the e^-e^- mode relative to the e^+e^- mode.[18]

In the above, effects of background have been neglected. The dominant background arises from imperfect beam polarization, and is $e^-\nu_e W^-$ with cross section $B = 43 \times 2P(1-P) + 400 \times (1-P)^2$ fb.[19] The beam polarization P is defined here as the fraction of right-handed electrons in each individual beam: $P = N(e_R^-)/[N(e_L^-) + N(e_R^-)]$. Polarizations of $P = 90\%$ are already available, and higher polarizations may be possible for future colliders.[20] For $P = 90\%$ (95%), the background is $B = 12$ (5) fb and is negligible, assuming it is well-understood and so contributes only to the the uncertainty through statistical fluctuations. While the difference between 90% and 95% polarization is not critical for this study, one might worry that the systematic uncertainty from beam polarization measurement might be significant. For example, to take an extreme case, if $P = 90 \pm 5\%$, the

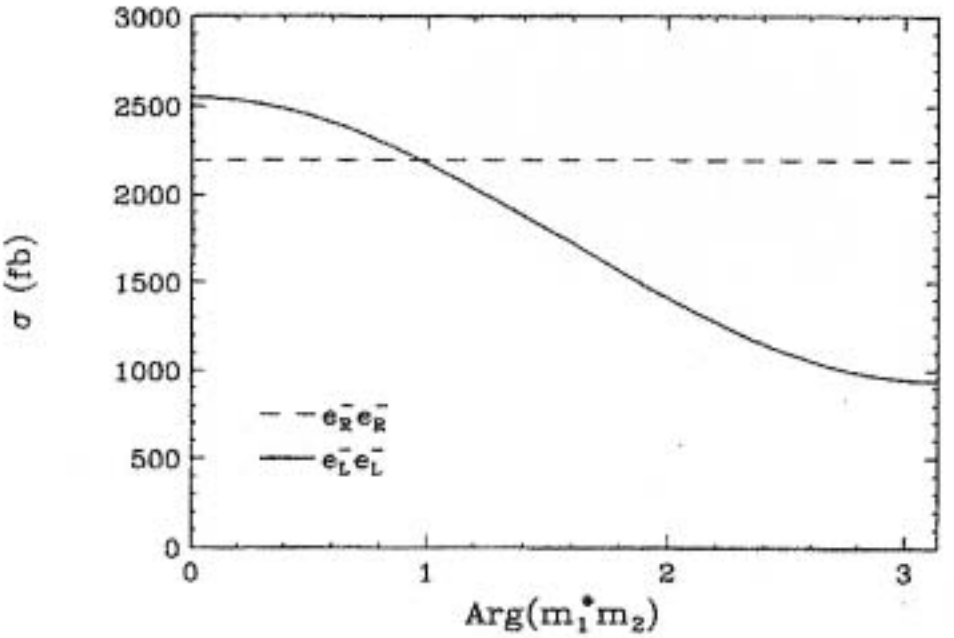

Fig. 1. Total cross sections for $e_R^- e_R^- \to \tilde{e}_R^- \tilde{e}_R^-$ and $e_L^- e_L^- \to \tilde{e}_L^- \tilde{e}_L^-$ in the pure gaugino or Higgsino limit as a function of $\mathrm{Arg}(m_1^* m_2)$. The parameters are $\sqrt{s} = 500$ GeV, $|m_1| = 100$ GeV, $|m_2| = 200$ GeV, $m_{\tilde{e}_R} = 130$ GeV, and $m_{\tilde{e}_L} = 180$ GeV. For reference $R \simeq 400$ fb at this center of mass energy.

and $\sigma(e_R^- e_R^- \to \tilde{e}_R^- \tilde{e}_R^-)$ are shown in Fig. 1 as a function of $\mathrm{Arg}(m_1^* m_2)$ with a typical set of parameters at the NLC. The differential cross sections for the same set of parameters are shown in Fig. 2. For constructive interference between bino and wino exchange in $e_L^- e_L^- \to \tilde{e}_L^- \tilde{e}_L^-$ the differential cross section is a monotonically increasing function of $\cos\theta$ in the forward hemisphere. Any non-monotonic deviation implies $\mathrm{Arg}(m_1^* m_2) \neq 0$. The sensitivity to $\mathrm{Arg}(m_1^* m_2)$ is very pronounced in the forward direction.

The large forward peak in both $e_R^- e_R^- \to \tilde{e}_R^- \tilde{e}_R^-$ and $e_L^- e_L^- \to \tilde{e}_L^- \tilde{e}_L^-$ is less pronounced for scattering near threshold, and with heavier neutralinos. The differential cross sections for slightly more massive states are shown in Fig. 3. For this set of parameters the $e_L^- e_L^- \to \tilde{e}_L^- \tilde{e}_L^-$ distribution is nearly flat in $\cos\theta$ for destructive interference.

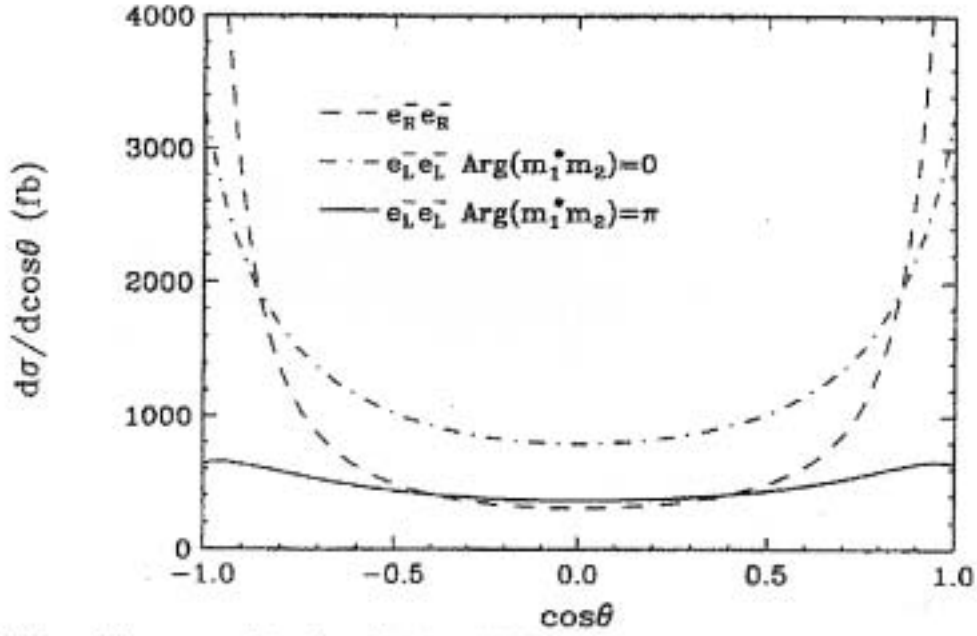

Fig. 2. Differential cross sections for $e_R^- e_R^- \to \tilde{e}_R^- \tilde{e}_R^-$ and $e_L^- e_L^- \to \tilde{e}_L^- \tilde{e}_L^-$ in the pure gaugino or Higgsino limit for $\mathrm{Arg}(m_1^* m_2) = 0, \pi$. The parameters are the same those in fig. 1.

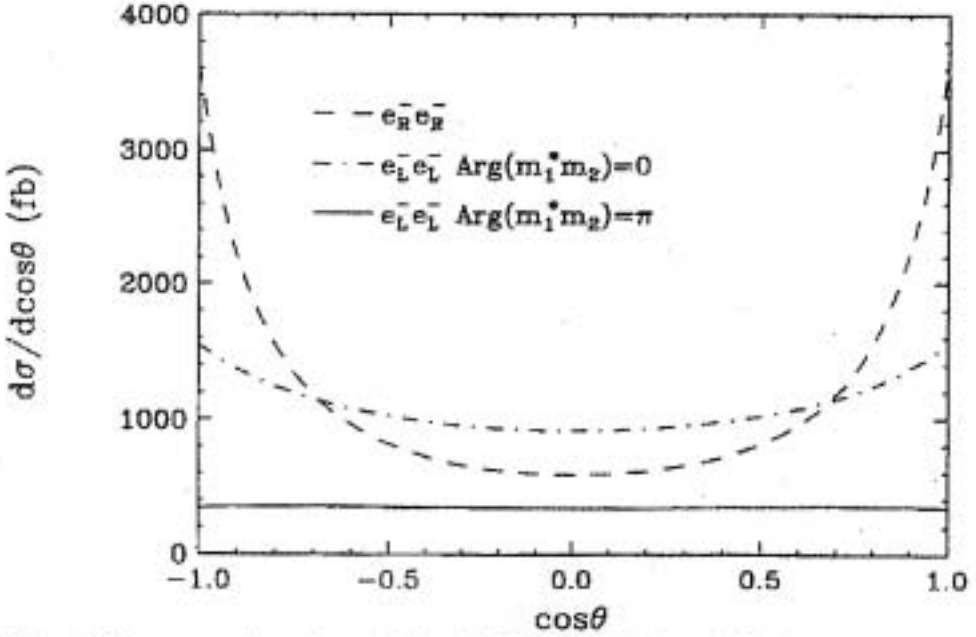

Fig. 3. Differential cross sections for $e_R^- e_R^- \to \tilde{e}_R^- \tilde{e}_R^-$ and $e_L^- e_L^- \to \tilde{e}_L^- \tilde{e}_L^-$ in the pure gaugino or Higgsino limit for $\mathrm{Arg}(m_1^* m_2) = 0, \pi$. The parameters are $\sqrt{s} = 500$ GeV, $|m_1| = 150$ GeV, $|m_2| = 300$ GeV, $m_{\tilde{e}_R} = 170$ GeV, and $m_{\tilde{e}_L} = 210$ GeV.